ISSN 0025-6544, Mechanics of Solids, 2019, Vol. 54, No. 6, pp. 903–914. © Allerton Press, Inc., 2019.
Russian Text © The Author(s), 2019, published in Izvestiya Akademii Nauk, Mekhanika Tverdogo Tela, 2019, No. 4, pp. 63–75.

Power Line Deformation Dynamics

R. Sh. Gimadiev*

Kazan State Power Engineering University,
ul. Krasnoselskaya 51, Kazan, 420066 Russia

Received September 12, 2018; revised September 12, 2018; accepted September 18, 2018

Abstract—A mathematical model of the dynamics of deformation of an overhead power line wire in a spatial setting is developed, the equations are solved on the basis of the finite difference method in an explicit scheme. In some cases, the accuracy of the calculations is compared with the obtained analytical solutions. A numerical study of the loading of a power line under the combined influence of wind and weight load was carried out. A numerical method for calculating wire breakage and the movement of parts after a break is proposed. The mechanism of the appearance of oscillatory motion such as "dancing wires" under the action of a variable wind load. The process of thermal conductivity and the dynamics of line deformation during melting of icing on wires by heating is studied, the transient processes of deformation of the power line are studied.

DOI: 10.3103/S0025654419060062

Keywords: *power line, deformation dynamics, numerical experiment, thermal conductivity, icing, wire dance.*

INTRODUCTION

Due to the relative cheapness of overhead power lines compared to cable ones and given the large distances, overhead lines (OHL) are widely used. Wires in OHL are subject to significant mechanical stress. They are constantly loaded with their own weight. Among the causes of additional mechanical loads, one can single out the effect of wind loads and icy-hoarfrost deposits. These reasons increase the load on the wires, and can also cause such dangerous forms of dynamic oscillatory processes as vibration and dancing wires. The wire dance effect is caused by a combination of weight and wind loads of a special profile. Mechanical loads can cause damage to power lines, which reduces the reliability of power supply and requires the cost of restoration of OHL.

To increase the reliability of OHL, standard technical solutions are used, and new technical solutions are proposed for studying the phenomenons of icing and wire dance and controlling them [1–4, 14–16].

The problem of studying mechanical damage to OHL, using both experimental and theoretical approaches to modeling loading processes, and finding methods to increase reliability is very relevant.

A number of works [5–10] are devoted to the theoretical study of mechanical loads on OHL, using various approaches to modeling the shape and tension in wires, they can be conditionally divided into two groups: 1) based on finite formulas, both without and with allowance for elongation wires 2) based on the numerical integration of the equations of motion.

The first group includes traditional approaches obtained under the assumption of static loading. The load due to the dead weight of the wire is considered evenly distributed. So in [4, 5] it is believed that the wire is inextensible and has the shape of a parabola (with a span of up to 800 m) or the shape of a chain line (with a span of more than 800 m). In [7], finite formulas were obtained for calculating the static stress-strain state of an OHL taking into account its tension. The advantage of these approaches is their ease of use. However, they do not allow to study the dynamics of the loading of OHL wires.

The second group of approaches to calculating the mechanical load of the overhead line allows you to study the dynamics of loading of the overhead line. These approaches are based on mathematical modeling of the movement of overhead wires under the action of loads using the equations of motion of an absolutely flexible system [5–10]. The equations of motion are nonlinear partial differential equations that are supplemented by initial and boundary conditions. This approach is associated with the compilation

*e-mail: gimadievr@mail.ru

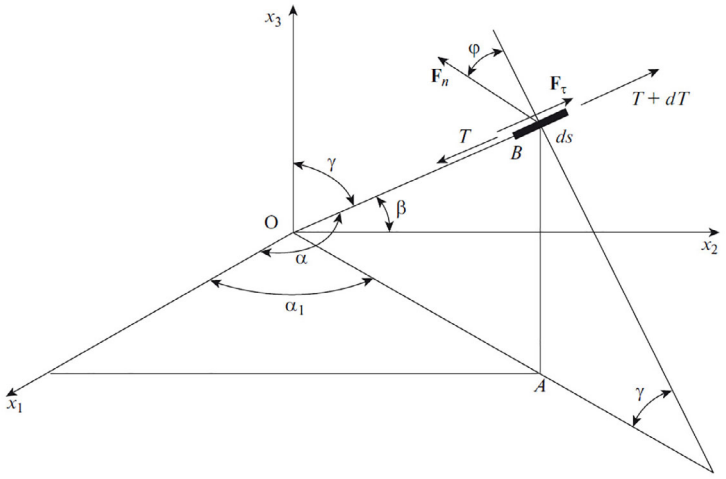

Fig. 1.

of a mathematical model, its programming, and numerical experiments. It is significantly more labor intensive than the first approach. The results of the first group of works can serve as tests for those programs.

It is of practical interest, on the basis of the developed models, to investigate the dynamic behavior of the wire under the influence of a combined weight and wind load, the deformation of the wire during the melting of icing by heating, and the behavior of OHL in the "wire dance" mode.

Low-frequency oscillations of overhead transmission lines were considered in [3, 14–16].

1. STATEMENT OF THE PROBLEM

The modeling of the dynamics of overhead transmission lines is carried out according to the model of an absolutely flexible system. By absolutely flexible systems we mean physical objects that neglect weak bending stresses, i.e. only work on tension and compression. These include: extended energy transmission lines, fiber-optic communication lines, cables located in the fluid flow [11], etc. The OHL supports are assumed to be absolutely rigid.

An absolutely flexible system in the field of gravity with a linear density $\rho_0(s)$, moves in space under the action of a distributed linear normal load F_n and a distributed linear tangent load F_τ. The deformation of a flexible system is characterized by the degree of elongation $\lambda = ds/ds_0 = 1 + e$, where ds_0 and ds are the lengths of the elements of the flexible system in an undeformed and deformed state, and e is the relative elongation. For an element of a flexible system with mass dm, in accordance with the law of conservation of mass, we have $dm = \rho_0 ds_0 = \rho ds$.

2. THE METHOD AND CONSTRUCTION OF THE SOLUTION

The vector equation describing the motion of an elastic weighty flexible system under the action of linear loads $\mathbf{F}_n$, $\mathbf{F}_\tau$, tension T, in the field of gravity with acceleration of gravity g has the form

$$\rho_0 \frac{\partial^2 \mathbf{r}}{\partial t^2} = \frac{\partial \mathbf{T}}{\partial s_0} + \mathbf{F}_n + \mathbf{F}_\tau + g\rho_0. \tag{2.1}$$

Let us consider the vector equation of motion in projections on the axis of the Cartesian coordinate system $x_1x_2x_3$, the acceleration g is directed down along the x_3 axis, Fig. 1.

Let the angle between the element ds of the flexible system and the coordinate axes Ox_1, Ox_2, Ox_3 be α, β, γ, respectively.

The distributed shear load with intensity $\mathbf{F}_\tau$ acts along the element ds of the flexible system. The effective normal load vector with intensity $\mathbf{F}_n$ makes an angle φ to the OAB plane. In addition, we introduce the angle α_1 between the Ox_1 axis and the OAB plane. Given that

$$|\mathbf{F}_n| = F_n, \quad |\mathbf{F}_\tau| = F_\tau, \quad |\mathbf{T}| = T, \quad |\mathbf{g}| = g, \quad \frac{\partial^2 \mathbf{r}}{\partial t^2} = \frac{\partial \mathbf{v}}{\partial t},$$

and projecting the vector equation of motion on the Cartesian coordinate axes, we have

$$\rho_0\frac{\partial v_1}{\partial t}=\frac{\partial}{\partial s_0}(T\cos\alpha)-F_n\lambda\cos\varphi\cos\gamma\cos\alpha_1+F_\tau\lambda\cos\alpha,$$
$$\rho_0\frac{\partial v_2}{\partial t}=\frac{\partial}{\partial s_0}(T\cos\beta)-F_n\lambda\cos\varphi\cos\gamma\sin\alpha_1+F_\tau\lambda\cos\beta,$$
$$\rho_0\frac{\partial\, v_3}{\partial\,\mathrm{t}}=\frac{\partial}{\partial s_0}(T\cos\lambda)+F_n\lambda\cos\varphi\sin\gamma+F_\tau\lambda\cos\gamma-\rho_0 g,$$

where v_1, v_2, v_3 are the projections of the speed of the elements on the coordinate axes.

Since $(\partial x_1)^2+(\partial x_2)^2+(\partial x_3)^2=(\lambda\partial s_0)^2$, then

$$\cos\alpha=\frac{1}{\lambda}\frac{\partial x_1}{\partial s_0},\quad \cos\beta=\frac{1}{\lambda}\frac{\partial x_2}{\partial s_0},\quad \cos\gamma=\frac{1}{\lambda}\frac{\partial x_3}{\partial s_0},$$
$$\tan\alpha_1=\frac{\partial x_2}{\partial x_1}=\Big(\frac{1}{\lambda}\frac{\partial x_2}{\partial s_0}\Big)\Big(\frac{1}{\lambda}\frac{\partial x_1}{\partial s_0}\Big)^{-1}=\frac{\cos\beta}{\cos\alpha},$$
$$\cos\alpha_1=\frac{\cos\alpha}{\sqrt{\cos^2\alpha+\cos^2\beta}},\quad \sin\alpha_1=\frac{\cos\beta}{\sqrt{\cos^2\alpha+\cos^2\beta}}.$$

In what follows, we omit the zero index in the s_0 coordinate and understand s as the Lagrangian coordinate (i.e., associated with a flexible system).

Given

$$\cos\alpha=\frac{1}{\lambda}\frac{\partial x_1}{\partial s},\quad \cos\beta=\frac{1}{\lambda}\frac{\partial x_2}{\partial s},\quad \cos\gamma=\frac{1}{\lambda}\frac{\partial x_3}{\partial s},$$

then the equations of motion of the flexible system in the Cartesian coordinate system $x_1x_2x_3$ will take the form

$$\begin{aligned}
\rho_0\frac{\partial v_1}{\partial t}&=\frac{\partial}{\partial s}\Big(\frac{T}{\lambda}\frac{\partial x_1}{\partial s}\Big)-F_n\cos\varphi\cos\alpha_1\frac{\partial x_3}{\partial s}+F_\tau\frac{\partial x_1}{\partial s},\\
\rho_0\frac{\partial v_2}{\partial t}&=\frac{\partial}{\partial s}\Big(\frac{T}{\lambda}\frac{\partial x_2}{\partial s}\Big)-F_n\cos\varphi\sin\alpha_1\frac{\partial x_3}{\partial s}+F_\tau\frac{\partial x_2}{\partial s},\\
\rho_0\frac{\partial v_3}{\partial t}&=\frac{\partial}{\partial s}\Big(\frac{T}{\lambda}\frac{\partial x_3}{\partial s}\Big)+F_n\lambda\cos\varphi\sin\gamma+F_\tau\frac{\partial x_3}{\partial s}-\rho_0 g.
\end{aligned}\tag{2.2}$$

The equations of motion in the vertical plane x_1x_2, the x_2 axis is directed vertically. In this case, for (2.2) we must assume

$$\alpha=\frac{\pi}{2},\quad \alpha_1=\frac{\pi}{2},\quad \gamma+\beta=\frac{\pi}{2},\quad \varphi=0,\quad \sin\gamma=\cos\beta=\frac{1}{\lambda}\frac{\partial x_2}{\partial s}$$

and replace the indices $2\to1$ and $3\to2$

$$\begin{aligned}
\rho_0\frac{\partial v_1}{\partial t}&=\frac{\partial}{\partial s}\Big(\frac{T}{\lambda}\frac{\partial x_1}{\partial s}\Big)-F_n\frac{\partial x_2}{\partial s}+F_\tau\frac{\partial x_1}{\partial s},\\
\rho_0\frac{\partial v_2}{\partial t}&=\frac{\partial}{\partial s}\Big(\frac{T}{\lambda}\frac{\partial x_2}{\partial s}\Big)+F_n\frac{\partial x_1}{\partial s}+F_\tau\frac{\partial x_2}{\partial s}-\rho_0 g,
\end{aligned}\tag{2.3}$$

where v_1 and v_2 are the projections of the velocity vector V on the x_1, x_2 coordinate axis.

The equations of motion (2.3) can also be written in compact form

$$\rho_{\mathrm{l}}\frac{\partial v_k}{\partial t}=\frac{\partial}{\partial s}\Big(\frac{T}{\lambda}\frac{\partial x_k}{\partial s}\Big)+(-1)^kF_n\frac{\partial x_{3-k}}{\partial s}+F_\tau\frac{\partial x_k}{\partial s}-\rho_{\mathrm{l}}g(k-1),\tag{2.4}$$

where $k=1,\ 2$; ρ_{l} is the linear density.

The components of the aerodynamic forces acting on a flexible system are determined by the equations [12]

$$F_n=\frac{\rho U_\infty^2}{2}d(c_{\mathrm{n}}\sin^2\alpha+c_\tau\sin\alpha),\quad F_\tau=\frac{\rho U_\infty^2}{2}dc_\tau\cos^2\alpha,\tag{2.5}$$

where U_∞ is the velocity of the unperturbed flow; ρ is the density of the medium; α is the angle of attack of an element of a flexible system; d is the conditional diameter; $c_n = 1.8446$, $c_\tau = 0.0554$ are aerodynamic flow coefficients, as for cables.

Transverse vibrations of flexible systems affect the normal components of linear efforts F_n: when the element of the flexible system moves against the flow, this component increases and decreases when it moves along the flow. With this in mind, the recount can be carried out according to the equation [13]

$$F_n(s,t) = F_n^0(s,t)\Big[1 - \mu\frac{V_n}{U_\infty}\Big]^2 \operatorname{sign}\Big[1 - \mu\frac{V_n}{U_\infty}\Big], \tag{2.6}$$

where V_n is the normal component of the velocity of an element of a flexible system; μ is the aerodynamic damping coefficient, this coefficient significantly affects the dynamics of loading.

The equations of motion (2.2) are solved in a dimensionless form by introducing the following dimensionless parameters:

$$\bar v_k = \frac{v_k}{U_\infty}, \quad f_n = 2\frac{F_n}{\rho U_\infty^2 L_0}, \quad f_\tau = 2\frac{F_\tau}{\rho U_\infty^2 L_0}, \quad \bar\rho = \rho\frac{L_0}{M_0},$$
$$\bar T = \frac{T}{T_0}, \quad \bar E = \frac{E}{T_0}, \quad \tau = t\frac{U_\infty}{L_0}, \quad \bar g = g\frac{L_0}{U_\infty^2},$$

where v_k is the speed of the wire element; L_0 is the wire span; $M_0 = \rho_0 L_0$ is the wire span mass; E is the reduced modulus of elasticity of the wire material; $T_0 = \rho U_\infty^2 L_0^2/2$ is the characteristic tension of the wire; t is the time; $A_N = \rho L_0^3/(2M_0)$ is the Newton parameter. Below in the notation, dashes over the parameters are omitted.

The equations are supplemented by the physical relations $T = T(e)$, $e \ge 0$ under tension and $e < 0$ under compression (in particular, with the linear law $T = Ee$), the kinematic relations

$$\frac{\partial x_k}{\partial \tau} = v_k, \tag{2.7}$$

and the geometric relation

$$\Big(\frac{\partial x_1}{\partial s}\Big)^2 + \Big(\frac{\partial x_2}{\partial s}\Big)^2 + \Big(\frac{\partial x_3}{\partial s}\Big)^2 = \lambda^2, \quad \lambda = 1 + e. \tag{2.8}$$

The initial and boundary conditions for the wire are written in the form

$$\begin{aligned} &x_k(0,s) = f_k(s), \quad v_k(0,s) = \varphi_k(s), \quad x_k(\tau,0) = f_k^\circ(\tau), \quad v_k(\tau,0) = \varphi_k^0(\tau),\\ &x_k(\tau,s_l) = f_{\mathrm{k}}^s(\tau), \quad v_k(\tau,s_l) = \varphi_k^s(\tau), \quad k = 1,\,2,\,3. \end{aligned} \tag{2.9}$$

3. THE DIFFERENCE SCHEME FOR SOLVING THE PROBLEM

The system of equations (2.2), (2.5)–(2.9) is solved by the finite difference method, a discrete region is introduced into consideration:

$$s_i = i\Delta s, \quad \tau_n = n\Delta\tau \quad (n = 0,\,1,\,\ldots,\tau/\Delta\tau - 1,\, i = 1,\,2,\,\ldots,\,s/\Delta s).$$

Using for approximation of derivatives the central differences on a grid shifted by a half step and an explicit finite-difference scheme, we can represent equations (2.2) in a dimensionless form as

$$
\begin{aligned}
v_{1,i}^{n+1/2} &= v_{1,i}^{n-1/2} + + \frac{\Delta\tau A_N}{\rho_0 \Delta s}\Big\{\Big[T_{i+1/2}^n \frac{x_{1,i+1}^n - x_{1,i}^n}{\Delta s \lambda_{i+1/2}^n} - T_{i-1/2}^n \frac{x_{1,1}^n - x_{1,i-1}^n}{\Delta s \lambda_{i-1/2}^n}\Big] \\
&\quad - \frac{1}{2\Delta s}\Big[(f_n)_{i+1/2}^{n-1/2}(x_{3,i+1}^n - x_{3,i}^n) + (f_n)_{i-1/2}^{n-1/2}(x_{3,i}^n - x_{3,i-1}^n)\Big]\cos\varphi\cos\alpha_1 \\
&\quad + \frac{1}{2\Delta s}\Big[(f_\tau)_{i+1/2}(x_{1,i+1}^n - x_{1,i}^n) + (f_\tau)_{i-1/2}^{n-1/2}(x_{1,i}^n - x_{1,i-1}^n)\Big]\Big\}, \\
v_{2,i}^{n+1/2} &= v_{2,i}^{n-1/2} + \frac{\Delta\tau A_N}{\rho_0 \Delta s}\Big\{\Big[T_{i+1/2}^n \frac{x_{2,i+1}^n - x_{2,i}^n}{\Delta s \lambda_{i+1/2}^n} - T_{i-1/2}^n \frac{x_{2,1}^n - x_{2,i-1}^n}{\Delta s \lambda_{i-1/2}^n}\Big] \\
&\quad - \frac{1}{2\Delta s}\Big[(f_n)_{i+1/2}^{n-1/2}(x_{3,i+1}^n - x_{3,i}^n) + (f_n)_{i-1/2}^{n-1/2}(x_{3,i}^n - x_{3,i-1}^n)\Big]\cos\varphi\sin\alpha_1 \\
&\quad + \frac{1}{2\Delta s}\Big[(f_\tau)_{i+1/2}^{n-1/2}(x_{2,i+1}^n - x_{2,i}^n) + (f_\tau)_{i-1/2}^{n-1/2}(x_{2,i}^n - x_{2,i-1}^n)\Big]\Big\}, \\
v_{3,i}^{n+1/2} &= v_{3,i}^{n-1/2} + \frac{\Delta\tau A_N}{\rho_0 \Delta s}\Big\{\Big[T_{i+1/2}^n \frac{x_{3,i+1}^n - x_{3,i}^n}{\Delta s \lambda_{i+1/2}^n} - T_{i-1/2}^n \frac{x_{3,1}^n - x_{3,i-1}^n}{\Delta s \lambda_{i-1/2}^n}\Big] \\
&\quad + \frac{1}{2}\Big[\lambda_{i+1/2}^n (f_n)_{i+1/2}^{n-1/2} + \lambda_{i-1/2}^n (f_n)_{i-1/2}^{n-1/2}\Big]\cos\varphi\sin\gamma \\
&\quad + \frac{1}{2\Delta s}\Big[(f_\tau)_{i+1/2}^{n-1/2}(x_{3,i+1}^n - x_{3,i}^n) + (f_\tau)_{i-1/2}^{n-1/2}(x_{3,i}^n - x_{3,i-1}^n)\Big]\Big\} - \Delta\tau \cdot g.
\end{aligned}
\tag{3.1}
$$

Here

$$
\cos\alpha = \frac{1}{2}\Big[\frac{x_{1,i+1}^n - x_{1,i}^n}{\Delta s \lambda_{i+1/2}^n} + \frac{x_{1,1}^n - x_{1,i-1}^n}{\Delta s \lambda_{i-1/2}^n}\Big], \quad \cos\beta = \frac{1}{2}\Big[\frac{x_{2,i+1}^n - x_{2,i}^n}{\Delta s \lambda_{i+1/2}^n} + \frac{x_{2,i}^n - x_{2,i-1}^n}{\Delta s \lambda_{i-1/2}^n}\Big],
$$

$$
\cos\gamma = \frac{1}{2}\Big[\frac{x_{3,i+1}^n - x_{3,i}^n}{\Delta s \lambda_{i+1/2}^n} + \frac{x_{3,i}^n - x_{3,i-1}^n}{\Delta s \lambda_{i-1/2}^n}\Big].
$$

The results of solving the problem at the integration step q serve as initial and boundary conditions for the next integration step.

An explicit computational scheme, along with advantage, also has a drawback: high-frequency oscillations of the solution appear behind the wave front. To smooth solutions, we use element velocity corrections:

$$
\bar{v}_k = v_k + \beta \frac{\partial^2 v_k}{\partial s^2}, \tag{3.2}
$$

where β is the velocity correction coefficient, which is selected on the basis of numerical experiments.

In the difference representation, the adjustment (3.2) has the form

$$
\bar{v}_{k,i}^{n+1/2} = v_{k,i}^{n+1/2} + \beta \frac{(v_{k,i+1}^{n+1/2} - 2v_{k,i}^{n+1/2} + v_{k,i-1}^{n+1/2})}{\Delta s^2}. \tag{3.3}
$$

The physical ratio is taken in the form of the Kelvin–Voigt equation

$$
T = E \cdot e + \eta \cdot \dot{e}, \tag{3.4}
$$

where $\dot{e}$ is the strain rate, η is the coefficient of internal friction in the material.

The OHL rupture occurs when the tension in element i at time τ_n exceeds the allowable rupture tension in material $T_i^n \geq [T]$, or rupture occurs as a result of mechanical damage. Let a line rupture occur in the element between the nodes i_l and $i_r = i_l + 1$, and the tension between these nodes instantly assumes a zero value of $T(i_l) = 0$. To calculate according to equation (3.1), we add an extended grid for the left span i_{l+1} and for the right span i_{r-1}, respectively

$$
v_{k,i_{l+1}}^{n+1/2} = v_{k,i_l}^{n+1/2}, \quad v_{k,i_{r-1}}^{n+1/2} = v_{k,i_r}^{n+1/2}. \tag{3.5}
$$

Thus, we obtain smooth solutions of the second derivatives for nodes (3.1) from $i = 2$ to $i = i_l$ for the left span and from $i = i_r$ to $i = \text{int}(s/\Delta s)$ for the right span.

The coordinates of the nodal points of the difference grid, or the kinematic relations are written in the form

$$x_{k,i}^{n+1} = x_{k,i}^{n} + \Delta\tau \bar{v}_{k,i}^{n+1/2}. \tag{3.6}$$

A necessary condition for the convergence of a numerical solution in an explicit scheme to the solution of a differential equation is the Courant–Friedrichs–Levy condition. For a material with a linear characteristic of elasticity E, this condition is written in the form $\Delta\tau \le \Delta s\sqrt{\rho_0/E}$, or

$$\Delta\tau = \alpha_k \Delta s \sqrt{\frac{\rho_0}{E}}, \tag{3.7}$$

where α_k is the Courant coefficient.

And so, end-to-end calculations are carried out according to equations (3.1)–(3.7). In the algorithm of a dynamic problem, the integration step (3.7) ensures the stability of the solution. Aerodynamic damping of the medium (2.6) and internal friction in the material (3.4) improve the stability of the numerical algorithm.

The equilibrium state of a flexible system is obtained as the ultimate solution to a dynamic problem. The choice of the coefficient of speed correction and the stability coefficient of the numerical solution is carried out by conducting numerical experiments on model problems. For numerical calculations of the OHL dynamics, one can use the results of modeling the dynamics of tape parachutes in a stream [13, p. 52–61]: the coefficient μ in the equation (2.6) is selected in the range of $0.1 \div 0.2$; and $\beta = (0.015 \div 0.03)\Delta s^2$ in equation (3.3) and $\alpha_k = (0.5 \div 1)$ in equation (3.7).

4. THE RESULTS OF TEST STUDIES

Let us consider separately the effect of wind load and weight force.

4.1. The Effect of Wind Load

A wind load of intensity p acts in the horizontal plane Ox_1x_2. The pressure drop due to wind acts normal to the deformable line and is evenly distributed. In this case, the deformed state of the line with two fixed ends is determined by the following approximate equations [11]

$$r = \frac{l}{2\sin\varphi}, \quad \varphi = \Big(\frac{3pl}{E}\Big)^{1/3}\Big[1 + \Big(\frac{3pl}{E}\Big)^{2/3}\frac{1}{60}\Big], \quad T = pr, \quad x_1 = r\Big[1 - \sqrt{1 - \Big(\frac{l}{2r}\Big)^2}\Big], \tag{4.1}$$

where l is the span; 2φ is the central angle of the circular arc; r is the radius of the circle; T is the tension; x_1 is the maximum deflection.

The relative error of the approximate solution (4.1) is:

$$\delta < 6\Big(\frac{\varphi^4}{7!}\Big)\Big(1 - \frac{\varphi^2}{20}\Big)^{-1}.$$

We use solution (4.1) for testing the effect of the wind load in numerical calculations.

Calculations according to (4.1): let the linear density of electric wires be $\rho = 0.5$ [kg/m], and the icing density $\rho_0 = \rho$. The total density is $\rho = 1.0$ [kg/m]; $l = 160$ [m]; $E = 80734 \cdot g$ [H] is the modulus of elasticity; wire diameter $d = 0.01553$ [m]; wind speed $V_\infty = 20$ m/c; linear wind load $p = \rho_a V_\infty^2 d/2$ [H/m^2]. Calculations according to (4.1) give: $\varphi = 0.132$; $r = 3.793$, $x_1 = 0.03309375$, and numerical calculations according to (3.1)–(3.7) at $\tau = 24.7$ give $x_1 = 0.03310$, Fig. 2, *a*. The relative error is less than $\theta = 0.007\,\%$. Moreover, the error of the most approximate solution does not exceed $\delta = 0.004 \times 10^{-2}\,\%$. Maximum deflection $x_1 = 0.0543$ at $\tau = 0.29$.

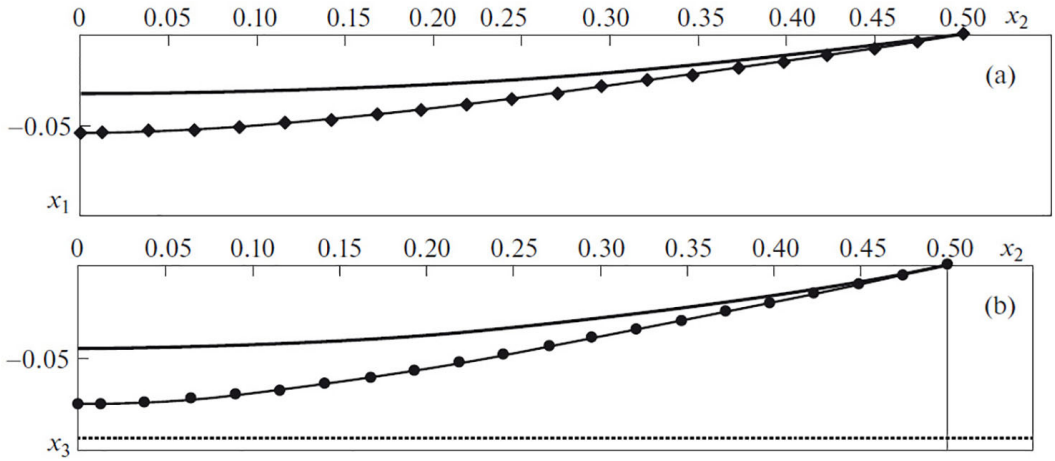

Fig. 2.

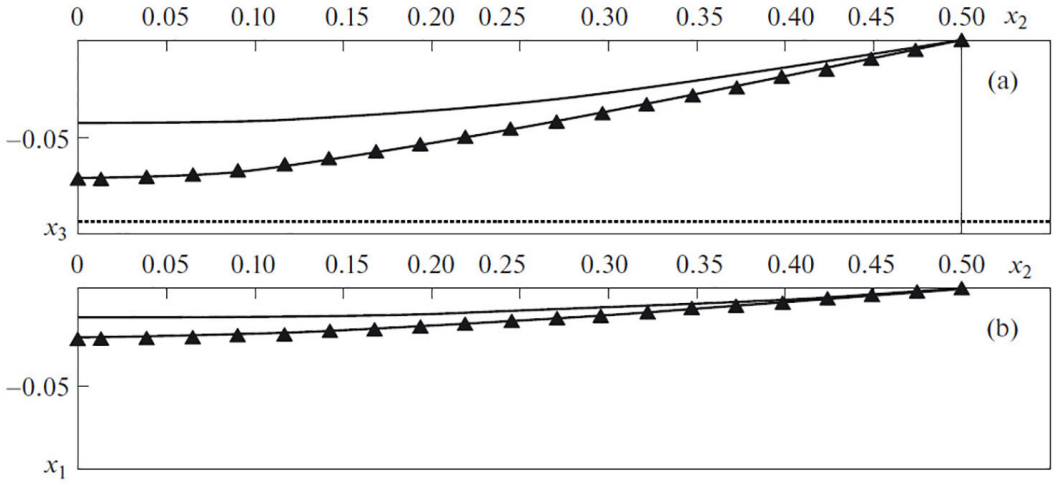

Fig. 3.

4.2. The Effect of Weight

And to analyze the accuracy of numerical calculations of the influence of weight, which acts along the Ox_3 axis in the Ox_2x_3 plane, we can use the solution [7]. The equation of the deformed chain line is determined by

$$x_3 = \rho_0 g \frac{1+\varepsilon}{E\varepsilon} \frac{x_2^2 - l x_2}{2}. \tag{4.2}$$

The maximum deflection in the middle of the span is

$$x_3 = -l^2 \rho_0 g \frac{1+\varepsilon}{E\varepsilon} \frac{1}{8}. \tag{4.3}$$

where the relative elongation is determined by the expression

$$\varepsilon = \sqrt[3]{\frac{\gamma}{2} + \left[\left(\frac{\gamma}{2}\right)^2 - \left(\frac{\gamma}{3}\right)^3\right]^{1/2}} + \sqrt[3]{\frac{\gamma}{2} - \left[\left(\frac{\gamma}{2}\right)^2 - \left(\frac{\gamma}{3}\right)^3\right]^{1/2}} \tag{4.4}$$

with the parameter $\gamma = (\rho_0 g)^2 l^2/(24E^2)$.

Calculations according to (4.3), (4.4) give $\gamma = 0.16365 \times 10^{-6}$ and $\varepsilon = 0.0054798$ and $x_3 = -0.04546$.

In Fig. 2, *b*, the calculations according to (3.1-3.7) $x_3 = -0.04540$ at time $\tau = 32.6$. In this case, the relative error of the error in comparison with the exact solution is $\theta \approx 0.12$ %. The maximum deflection $x_3 = 0.0753$ is realized at time $\tau = 0.21$.

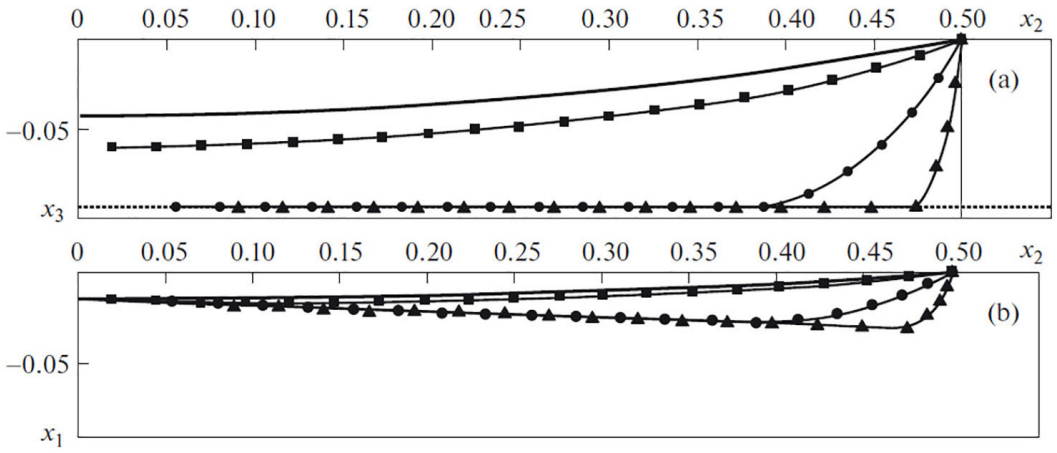

Fig. 4.

4.3. Calculation of the Spatial Shape of OHL Under the Influence of a Combined Wind and Weight Load

We will take the initial state of the flexible system at time $\tau = 0$ in the form of a straight line (which approaches the optimal weight of the OHL). From this state, the system is deformed to the value of maximum deflections in the vertical plane $x_3 = -0.0717$ (Fig. 3, *a*) and $x_1 = -0.0279$ in the horizontal plane (Fig. 3, *b*) at time $\tau = 0.204$. After time $\tau = 40.75$, the system reaches an equilibrium state and the maximum deflections are $x_3 = -0.0433$ and $x_1 = -0.0169$, Figs. 3, *a, b*.

4.4. OHL Movements after a Gap in the Middle of the Span.

In the algorithm for calculating the overhead line movement after a break, the following assumptions are used: a) for a steady mode of influence of wind and weight load, wire breakage, for example, occurs in the middle of the span; b) at the moment of falling to the ground, the influence of the wind load on the wire ceases; c) when falling to the ground, a partially elastic impact occurs and it is assumed in the calculations that the kinetic energy of the rebound is 36% of the energy of the vertical impact. Figs. 4, *a, b* shows the results of calculating the movement after a wire break in the middle of the span at time instants $\tau = 40.85;\ 41.87;\ 50.93$.

4.5. The Effect of a Gust of Wind.

Low-frequency oscillations of OHL (frequencies of the order of 1 Hz) occur due to a gust of wind. Oscillations can occur with an amplitude above a meter [14], [15], [16]. In these works, it is noted that the mechanism for the appearance of oscillations is not always clear.

Consider a gust of wind that acts in the horizontal plane Ox_1x_2 with a sinusoidal law of change

$$p(\tau) = q_0 d \left| \sin\left(\frac{\pi n}{\delta}\right)\right|, \tag{4.5}$$

where q_0 is the pressure head at wind speed V_0, d is the diameter of the wire, $n = \tau/\Delta\tau$, τ is the current time, $\Delta\tau$ is the integration step, $n/\delta = 1,\ 2,\ 3,\ \ldots$ are the zeros of the sine wave.

In Fig. 5, *a, b, d*, the results of calculating the movement of the midpoint of the span in accordance with the algorithm (3.1)–(3.7) are presented. The initial state of the span at time $\tau = 0$ is taken as a straight line. From this state, under the influence of the weight of the wire, a transition process is realized to the form of an equilibrium state (Fig. 5, *a*). The maximum deflection is $x_3 = -4.54 \times 10^{-2}$. At time $\tau = 4$, a gust of wind acts in accordance with (4.5). Oscillations of the midpoint of the wire are given in the horizontal plane, Fig. 5, *b*.

Consider the following option, the wind pressure changes according to the law (4.5) at time $\tau \geq 4$ and coincides with the movement at the speed of the wire elements $\nu_{x_{1i}} \leq 0$, and with the movement of the wire element $\nu_{x_{1i}} > 0$ it is zero. That is, a gust of wind contributes to the swaying of the wire in the horizontal plane Ox_1x_2. These calculation results are shown in Fig. 5, d. The amplitude of oscillation in the Ox_1x_2 plane increases. These vibrations are reflected in the vibrations of the wire in the vertical plane Ox_2x_3 and the occurrence of vibrations such as "dancing wires".

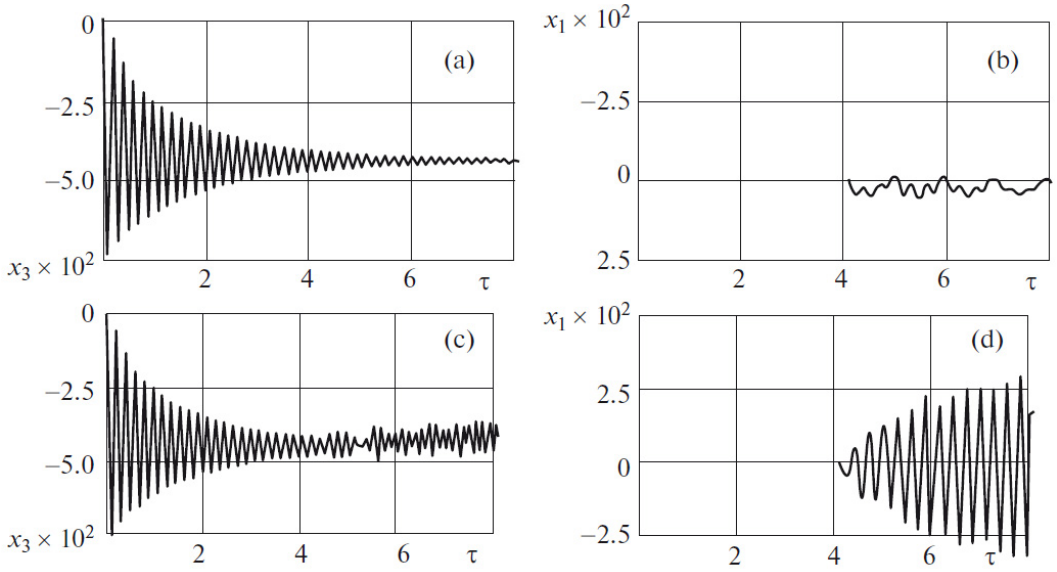

Fig. 5.

5. THE THERMOELASTIC PROBLEM OF OHL

In the autumn-winter-spring period, favorable conditions are created for the formation of ice deposits on power lines. To combat this dangerous phenomenon, various technologies are developed and used, including those based on heating wires to melt ice [1, 2].

With the formation of ice, the mass of the wire increases and the system goes into a new equilibrium deformed state. When the heating is turned on, the wire sags even more due to temperature elongation. After warming up, the icing is dropped, the temperature drops to ambient temperature, and the shape of the wire goes back to equilibrium, which corresponds to loading only by the weight of the wire itself.

5.1. The Dimensionless Heat Equation

The dimensionless heat equation for a linear element has the form

$$u_t = u_{ss} + f, \tag{5.1}$$

where $0 < s < 1$, $0 < t < t_k$, f is the density of heat sources.

5.2. The Heat Equation in the Difference Representation

Let $\varphi_i^j = f_i^j$, $s_i = i \cdot h$, $i = 0, 1, 2, \ldots, N$, $h = 1/N$ be the step of the partition along the Lagrangian coordinate, N be the number of partitions of the span, $t_i = j \cdot \tau$, $j = 0, 1, 2, \ldots, L$, $\tau = t_k/L$ be the step of integration over time, and L be the number of partitions of the time interval. For (5.1) we have

$$u_i^{j+1} = \left(1 - 2\frac{\tau}{h^2}\right)u_i^j + \frac{\tau}{h^2}(u_{i+1}^j + u_i^j) + \tau\varphi_i^j. \tag{5.2}$$

The stability of the circuit in the grid norm for the integration step requires the fulfillment of the condition $\tau = \alpha h^2/2$, $0 < \alpha \leq 1$.

5.3. Approximation of Boundary Conditions

Approximation can be carried out in two ways. Option 1. To approximate the boundary conditions, we use the quadratic Lagrange polynomial over three points of the segment. For the first time derivatives at the ends of the segment, we have

$$u_{0\tau}^{(1)} = \frac{1}{2\tau}(-3u_0^{j+1} + 4u_1^j - u_2^j), \quad u_{N\tau}^{(1)} = \frac{1}{2\tau}(3u_N^{j+1} + 4u_{N-1}^j - u_{N-2}^j).$$

And for the second derivatives with respect to the coordinate at the borders, we have

$$u_{0h}^{(2)} = \frac{1}{h^2}(u_0^j - 2u_1^j + u_2^j), \quad u_{Nh}^{(2)} = \frac{1}{h^2}(u_N^j - 2u_{N-1}^j + u_{N-2}^j).$$

Then for the boundaries at the integration step $(j+1)$ we have

$$\begin{aligned} u_0^{j+1} &= -\frac{2\tau}{3h^2}u_0^j + \frac{4}{3}(1+\frac{\tau}{h^2})u_1^j - \frac{1}{3}(1+2\frac{\tau}{h^2})u_2^j + 2\tau\varphi_i^j, \\ u_N^{j+1} &= \frac{2\tau}{3h^2}u_N^j + \frac{4}{3}(1-\frac{\tau}{h^2})u_{N-1}^j - \frac{1}{3}(1-2\frac{\tau}{h^2})u_{N-2}^j + 2\tau\varphi_i^j. \end{aligned} \tag{5.3}$$

Option 2. For the boundaries, we use the linear approximation

$$\begin{aligned} u_0^{j+1} &= (1+2\frac{\tau}{h^2})u_0^j + \frac{\tau}{h^2}(u_2^j - 2u_1^j) + \tau\varphi_0^j, \\ u_N^{j+1} &= (1+2\frac{\tau}{h^2})u_N^j + \frac{\tau}{h^2}(u_{N-2}^j - 2u_{N-1}^j) + \tau\varphi_N^j. \end{aligned} \tag{5.4}$$

5.4. Test Calculations of Thermal Conductivity Using Both Options

For calculations, we take the following initial data: initial wire length $l = 160$ [m]; the linear expansion coefficient of the aluminum wire is $\alpha_t = 23.8 \times 10^{-6}$ [1/K]; elasticity modulus $E = 6.25 \times 10^{10}$ [H/m^2] [4]; wire diameter $d = 0.0147$ [m]; wire material density $\rho = 2700$ [kg/m^3]; thermal capacity of mass unit $c = 0.9$ [kJ/(kg K)]; thermal conductivity coefficient $k = 209$ [Vt/(m K)]; K is the Kelvin temperature. The number of elements $N = 50$.

The insulated wire is divided into two parts. Instantly the left span is heated to 200° C (473.15 K), and the right span has ambient temperature of minus 5° C. In a dimensionless form, these temperatures will be 1.7322 and 0.9817. The redistribution of temperature along the length and time occurs without heat loss and the process continues to the temperature of equalization to $(1.7322 + 0.9817) \times 0.5 = 1.35695$, which corresponds to 370.65089 K.

Heat conductivity calculations are carried out according to (5.2) when approximating the boundary conditions according to option 1 and option 2 and compare with the exact value 1.35695.

According to option 1 (approximation of the boundary conditions by a quadratic Lagrange polynomial), a numerical calculation gives an equalization temperature of 1.36058 in 2.3 s.

For option 2 (linear approximation of the boundary conditions), the calculation gives 1.35689. Option 2 gives the best convergence.

5.5. Linear Thermal Expansion

The relative thermal expansion is

$$\varepsilon_t = \frac{l_2 - l_1}{l_1} = \alpha_t \Delta u, \tag{5.5}$$

where l_1 and l_2 are the initial and final lengths of the wire, and $\Delta u = u_2 - u_1$ is the temperature difference, α_t is the coefficient of linear expansion. The force arising in the wire due to thermal expansion is determined by

$$T = E\varepsilon_t \frac{\pi d^2}{4}. \tag{5.6}$$

Calculations based on the above accepted initial data give: relative thermal elongation $\varepsilon_t = 24.4 \times 10^{-4}$, the force arising in the wire due to thermal elongation, respectively, $T = 25.9$ kN.

5.6. OHL Dynamics Taking into Account the Weight of the Wire, the Weight of Icing and Thermal Conductivity

For example, let the icing density be equal to the density of the wire itself $\rho_0 = \rho$, in practice it can exceed it by several times. In accordance with the solution of the equation of motion, the wire under the action of only its own weight at time $t = 2.7$ moves to the maximum deflection $x_3 = 3.4$ m

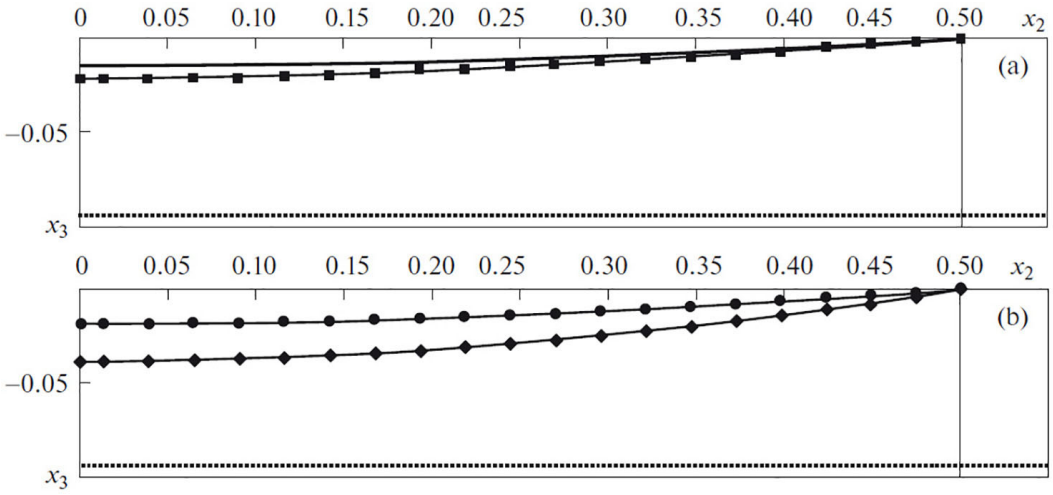

Fig. 6.

(Fig. 6, a, line −■− , $x_3 = 0.021253$), while the tension is $T = 12$ kN, then as a result of the transition process after about 30 seconds self-settles to the form of an equilibrium state with a maximum deflection $x_3 = 2.3 (x_3 = 0.01438)$. A uniform mass of icing is superimposed on this form of the equilibrium state. The system again reaches an equilibrium state with a mass of wire and icing; this state at time $t = 51$ is shown in Fig. 6, *b* (line −•−). In this case, the maximum deflection is $x_3 = 2.95$ m ($x_3 = 0.01844$) and tension $T = 9.8$. It is believed that at time $t = 51$, $1/10$ of the span is instantly heated to a temperature of 150° C, and this temperature is kept constant on this part and heats the rest of the span due to thermal conductivity for 5 seconds. During this time, this temperature has time to spread and even out to 150° C along the entire length. In this case, elongation occurs due to thermal expansion, Fig. 6, *b* (line −◇−). At the end of heating, the deflection reaches $x_3 = 6.20$ m ($x_3 = 0.03875$), and the temperature tension in the wire is 38.

After that, the mass of icing is considered to be dropped immediately and within one second the temperature is equalized with the ambient temperature equal to minus 5° C. Further movement is calculated, the system goes into a new equilibrium state with a maximum deflection $x_3 = 2.3$ m ($x_3 = 0.01438$) and a tension in the wire of 6.2 kN (this equilibrium state is shown in Fig. 6, *a* by a solid line).

Note that a change in temperature over time is associated with the rate of change of temperature, and a change in the movement of wire elements is associated with acceleration. Therefore, at the end of the heating of the wire, the temperature is distributed almost uniformly along the length of the wire, and the elastic elongations along the length are unsteady in nature, the elastic tension only aligns over time. Therefore, at the end of heating, only the temperature tension can be more accurately estimated.

6. CONCLUSION

The equations of motion of a deformable power line in a spatial setting are obtained. A method for calculating the dynamics of a power line in a spatial setting is developed. Numerical studies of OHL loading by weight, wind and icing load were carried out. A method for calculating wire breakage and the movement of parts after a breakage is proposed. A method has been developed for calculating the thermoelastic problem during icing and melting of OHL. The mechanism of the appearance of oscillatory motion such as "dancing wire" under the action of a variable wind load. The reliability of numerical calculations for particular cases is verified by the obtained analytical solutions.

REFERENCES

1. R. G. Minullin and I. Sh. Fardiev, *Locational Diagnostics of Overhead Power Lines* (Kaz. Gos. En. Univ., Kazan, 2008) [in Russian].
2. G. G. Ugarov, A. A. Kolesnikov, and V. Ya. Bashkevich, "Synthesis of a Control System for Smelting Deposits on Overhead Power Lines Equipped with an Information-Measuring System," Vest. Sarat. Gos. Tekh. Univ. **3** (1), 120–128 (2008).

3. E. V. Shevchenko and T. E. Udod, "Development of Methods for Combating OHL Dance Wires for Ukraine," Met. Konst. **12** (4), 239–247 (2006).
4. N. L. Baceva, *Special Issues in Designing Electric Power Systems and Networks: A Tutorial* (Tomsk Pol. Univ., Tomsk, 2008) [in Russian].
5. E. V. Shevchenko, V.A.Mitrakov, and A.V.Tanasoglo, "Determination of Reduced Tension in Case of Wire Break," Met. Konst. **16** (3), 189–198 (2010).
6. A. I. Sokolov, "Nonlinear Vibrations of an Absolutely Flexible Eire in the Air Stream," Nauka Obraz., No. 4–1, 5 (2008)
7. R. Sh. Gimadiev, F. F. Dinmukhametov, and N. R. Galimullin, "Calculation of the Spatial Dynamics of Overhead Lines under the Combined Influence of Wind and Weight Load," Izv. VUZov Probl. Energ., No. 3–4, 28–37 (2010).
8. R. Sh. Gimadiev and F. F. Dinmukhametov, "Modeling the Breakdown of Energy Transmission Lines," Izv. VUZov Probl. Energ., No. 7–8, 137–143 (2008).
9. R. Sh. Gimadiev and T. Z. Gimadieva, "Mathematical Modeling of Power Line Deformation Taking Into Account Thermal Conductivity," Izv. VUZov Probl. Energ., No. 9, 51–59 (2011).
10. R. Sh. Gimadiev, "The Problem of Thermoelasticity of Power Lines," in *Abstracts of the 8th Int. Scientific and Technical Conf. "Innovative Engineering Technologies, Equipment and Materials 2017", Kazan,* (Kazan, 2017), Vol. 2, pp, 141–145.
11. R. Sh. Gimadiev, Ilgamov M.A. "Static Interaction of Soft Wing Profile with Incompressible Fluid Flow," Izv. VUZov Aviaz. Tekh., No. 1, 43–48 (1998).
12. S. I. Devnin, Hydroelasticity of Structures During Tear-Off Flow (Sudostroyeniye, Leningrad, 1975) [in Russian].
13. R. Sh. Gimadiev, Parachute-Type Soft Shell Dynamics (Kaz. Gos. En. Univ., Kazan, 2006) [in Russian].
14. J. McCombe and F. R. Haigh, *Overhead Line Practice* 3rd ed. (Macdonald, 1966), pp. 216–219.
15. H. M. Ryan, *High Voltage Engineering and Testing*, (IET, 2001), p. 192.
16. A. J. Pansini, *Power Transmission and Distribution* (The Fairmont Press, Inc., Lilburn, 2004), pp. 204–205.